



pubs.acs.org/acsaenm

Robust, Reproducible Silica Scaffold for Liquid Flow Applications

Rebecca G. Davies, Allyson E. MacInnis, Patrick J. Bisson, and Mary Jane Shultz*



Cite This: ACS Appl. Eng. Mater. 2023, 1, 1752-1758



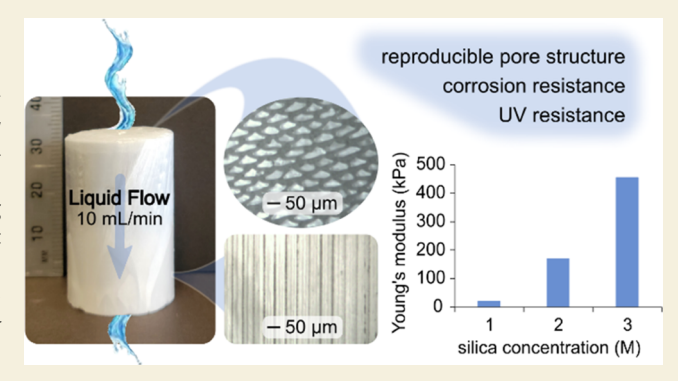
ACCESS I

Metrics & More

Article Recommendations

Supporting Information

ABSTRACT: A high-deposition-area, robust inorganic scaffold, unique in its reproducible anisotropic macropores, is reported. This scaffold has a Young's modulus of 455 \pm 34 kPa and a yield strength of 215 \pm 10 kPa in compression. It supports 3.5 \pm 1.0 mL min⁻¹ cm⁻² volumetric flux of water with a modest 4.4 kPa head pressure. The scaffold is generated by freeze-casting a low-pH, concentrated silicic acid solution, followed by supercritical drying (SCD), changing the way water glass is used to generate support substrates. The scaffold enables facile immobilization of molecules or nanoparticles for liquid-phase applications, including heterogeneous catalysis, separations, biomedical devices, and energy storage.



KEYWORDS: freeze-casting, supercritical drying, monolith, reproducible macropores, liquid flow, degradation-resistant, mechanically robust

■ INTRODUCTION

Meso- and macroporous^{1,2} siliceous materials have been studied extensively for use in diverse applications for over 20 years. They show promise in areas as diverse as heterogeneous catalysis, 3,4 energy storage, 5 adsorption and separations, 6-8 and biomedical devices. 9-11 These siliceous materials are synthesized in a wide range of morphologies and by several processes to meet the diverse physical and chemical requirements of these applications. Common materials include composites, 4-6,12,13 aerogels and xerogels, 8,10,14,15 films and membranes, 7,16 particles, 17 and microstructured monoliths. 3,18-20 Preparation methods include sol-gel processing, 3,14,21 templating methods, 4,8,10,19,20,22 deposition, and a variety of other techniques.

Among the reported siliceous materials,²² most target solid gas applications such as heterogeneous catalysis or adsorption. Synthesis methods for materials targeting solid-gas applications often focus on maximizing surface area with little consideration of mechanical strength. In contrast, liquid flow applications favor micron-scale pores to reduce head pressure requirements resulting from Laplace pressure and good mechanical strength for robustness through multiple flow cycles. Of monoliths reported for liquid-phase applications, most include organic linkages integral to maintaining monolith structure. ^{2,3,10,12,13,16,18,23–26} In many applications, a purely inorganic scaffold may be preferable for resistance to corrosion or catalytic degradation.

This contribution describes a mechanically robust, degradation-resistant, highly reproducible, and anisotropically macroporous silica scaffold for liquid flow applications. This ordered silica monolith is easily prepared by freeze-casting and supercritical drying of a sol prepared from commercially available sodium metasilicate solution. The purely inorganic backbone prevents degradation that may result from unintended reaction with adsorbed moieties. Through freezecasting, 65 μ m \times 30 μ m diameter pores with approximately 10 μm thick walls are generated, creating a large deposition-areato-volume ratio while allowing passage of significant liquid volumes with low head pressure. This large pore scaffold morphology is desirable for low energy consumption, moderate head pressure, and long-term applications. Due to the high surface tension (γ) of water, ideal pore sizes for lowpressure aqueous flow exceed 10 microns. Per the Laplace-Young equation,²⁷ pores on the order of 10–100 μ m diameter $(5-50 \mu \text{m radii}, R)$ correspond to pressures (p) of 0.3 to 0.03 atm for water:

$$\Delta p = -\gamma \left(\frac{1}{R_1} + \frac{1}{R_2} \right) \tag{1}$$

Scaffolds generated by this method allow $3.5 \pm 1.0 \text{ mL min}^{-1}$ cm⁻² volumetric flux at 4.4 kPa head pressure and have a Young's modulus of 455 ± 34 kPa in compression. The translucency of the silica scaffold lends itself to applications where adsorbed moieties are activated by visible and UV light.

Received: March 29, 2023 Revised: June 5, 2023 Accepted: June 5, 2023 Published: June 20, 2023





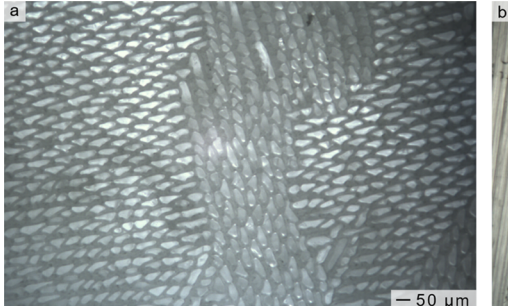




Figure 1. Micrographs of (a) a transverse section and (b) a longitudinal section of a frozen three-molar precursor scaffold. Regions of lighter coloration indicate the presence of ice, and darker regions indicate grain boundaries within the silica scaffold. The semi-horizontal line in the top third of Figure 1b is an artifact of the microtome blade used to prepare the section. Micrographs are collected at -20 °C and atmospheric pressure.

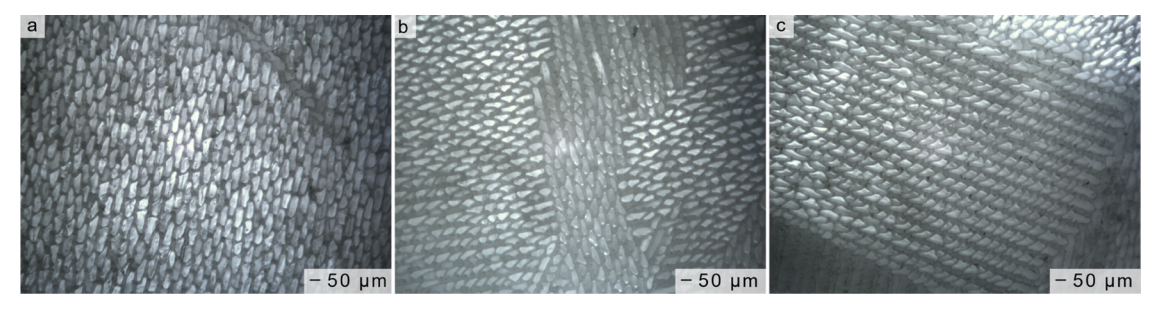


Figure 2. Micrographs of transverse cuts from the (a) top, (b) middle, and (c) bottom of the scaffold shown in Figure 1, demonstrating consistent microstructure throughout the length of the scaffold. There is no correlation in the positioning of the sample between cross-sectional images.

EXPERIMENTAL SECTION

Scaffold Synthesis

One-molar sodium metasilicate solution (50 mL, Sigma-Aldrich) was run through a column containing Amberlite IR120 hydrogen form ion exchange resin (125 mL, Supelco). Low-pH (1–2) silicic acid solution effluent (50 mL) was rotary evaporated to a three-molar concentration. The concentrated, low-pH effluent was poured into a cylindrical Teflon mold (2.54 cm. I.D. \times 5.08 cm height) with a copper plug bottom, and the copper plug was dipped directly into liquid nitrogen to freeze unidirectionally, or freeze-cast, until solidified. Liquid nitrogen was manually replenished to maintain copper plug contact with the liquid nitrogen surface for the duration of the freeze-cast. The frozen scaffold was moved to a $-20\,^{\circ}\mathrm{C}$ freezer for 24 h.

Microscopy

Transverse and longitudinal scaffold sections were saw-cut, microtomed, and slide-mounted in the frozen state. Images were collected using a Meiji compound microscope (4× objective) and PixeLINK PL-A662 Megapixel FireWire Camera (mounted atop the 0.7× magnification photo tube). Average grain size was analyzed using ImageJ and calibrated scale bars.

Supercritical Drying

Frozen scaffolds were submerged in 100 mL of room-temperature ethanol for 24 h, and the ethanol was exchanged twice more for 24 h each. The ethanol-exchanged scaffold was loaded into a custom SCD (supercritical drying) cell with 70 mL of ethanol and sealed. The cell was heated and held above the critical point of ethanol (241 $^{\circ}$ C, 62.2 atm) for 5 min. Pressure was vented over 2 min, and the cell cooled to room temperature.

Uniaxial Strain

A uniaxial stress—strain apparatus was constructed according to Genov's description.²⁷ Supercritically dried scaffolds of known dimensions were placed atop a Radwag WLC X2 Precision Balance (20 kg max) or an Accuteck A-BC200 Digital Scale (98 kg max), and the balance was zeroed. The lab jack and plate supporting the scale

were raised until touching the pin of the Teclock drop dial indicator and mass registered on the balance. Mass was recorded as a function of displacement until the scaffold fractured.

Flow

A flow apparatus was glass-blown from a 2.54 cm diameter glass tube with overflow ports at various heights (15, 28, and 45 cm) from the top of the scaffold. Three-molar scaffolds were heat-shrink-wrapped to the bottom of the flow apparatus, allowing only longitudinal liquid flow. Two overflow ports were plugged, so only one head pressure was probed at a time. Reserve water was added continuously to the apparatus as water flowed through the scaffold and out of the unplugged overflow port, maintaining a constant head pressure throughout flow characterization. Effluent volumes were recorded as a function of time.

RESULTS

Freeze-Casting and Supercritical Drying

During freeze-casting, solidifying water sweeps solutes to the grain boundaries, generating a silica scaffold precursor. During aging, acid-catalyzed condensation consolidates silica walls, giving rise to closed and continuous anisotropic pores (Figure 1).^{2,28} The choice of sodium silicate starting material ensures inexpensive manufacture of scaffolds resistant to corrosion and UV degradation. An ion exchange resin was utilized to both lower pH and remove sodium cations which act as flocculating agents, causing premature gelation.²⁹

Grain size measurements reveal average pore cross-sectional widths of $55-75~\mu m$ by $25-35~\mu m$: an aspect ratio of approximately 2:1. Average pore size is controlled by adjusting the freeze-cast temperature (Table S1 and Figure S1). Freezing at $-196~^{\circ}$ C prevents settling of silicic acid oligomers (Figure S2) during the freeze-cast, yielding highly reproducible pore structures, both longitudinally and transversely. Pore cross section (Figure 2) remains consistent along the entire height of the sample (approximately $3.8~\pm~0.1~cm$).

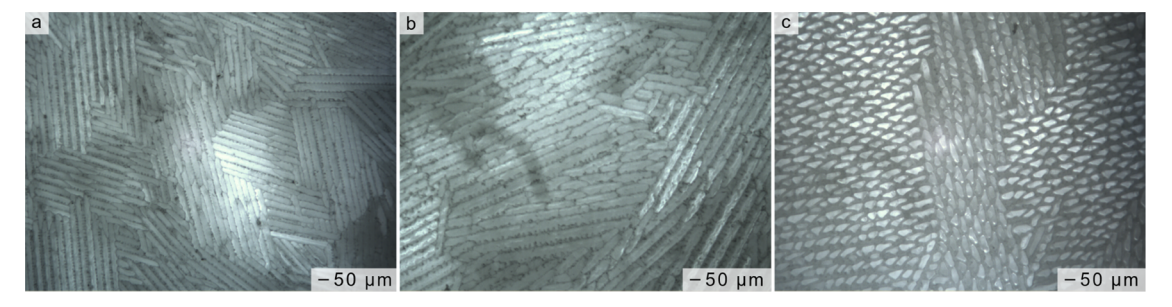


Figure 3. Scaffold transverse cut micrographs of (a) one-, (b) two-, and (c) three-molar silica concentrations. Below three-molar silica concentration, pores are inconsistent in size and shape, with many lamellar structures lacking cross-connections. Because of this lack of reproducible pore structure, average pore size measurements for one- and two-molar scaffolds are not meaningful nor reported.



Figure 4. (a) Photograph of a completed scaffold after removal from SCD cell. Longitudinal micron-scale pores are visible from the dried scaffold exterior. The ruler is present as a guide to the eye; each three-molar scaffold is approximately 3.8 ± 0.1 cm in height. (b) Photograph of the supercritical drying cell inside a heating mantle. During SCD, input voltage is controlled, and pressure and temperature are monitored.

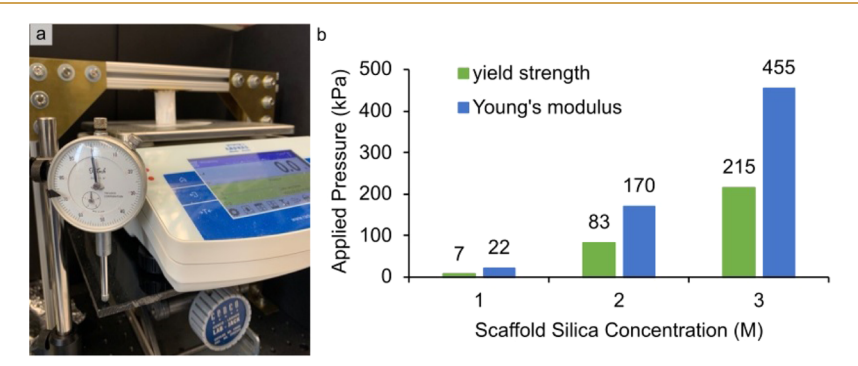


Figure 5. (a) Photograph of stress—strain compression testing apparatus with scaffold. (b) Measurements of silica scaffold yield strength and Young's modulus in compression as a function of concentration. Yield strengths of one-, two-, and three-molar scaffolds were 6.8 ± 2.6 , 83 ± 13 , and 215 ± 10 kPa, respectively; Young's moduli were 22 ± 13 , 170 ± 14 , and 455 ± 34 kPa. Reported values were averaged from three scaffold compression measurements. Each increase in silicic acid concentration yields a corresponding increase in compressive strength.

To optimize scaffold strength, scaffolds with one-, two-, and three-molar silicic acid concentrations were synthesized and subjected to compression measurement (Figure S3). Consistently, frozen-state scaffold cross sections (Figure 3) reveal that fully consolidated walls are only observed at the three-molar concentration. Below three-molar, the scaffold shows many lamellar structures, lacking cross-connections.

Supercritical drying (SCD) was used to remove water without damaging the scaffold pore structure, transforming scaffolds from the frozen state to a dry, usable product (Figure 4a). The SCD cell is shown in Figure 4b. When supercritically drying scaffolds, ethanol is used as the solvent; it has a much

lower surface tension (22.32 mN/m) than does water (72 mN/m), thus putting less strain on the nascent scaffold. Additionally, supercritical conditions for ethanol are milder than those for water. Keeping ethanol above its critical point, venting pressure at high temperature, and lowering temperature allows the scaffold to avoid a harsh liquid-to-gas phase transition. This preserves the pore structure and minimizes shrinkage in contrast to calcination, which collapses pores.³¹ Supercritical drying offers a significant increase in compressive strength of scaffolds compared to lyophilization and air-drying.

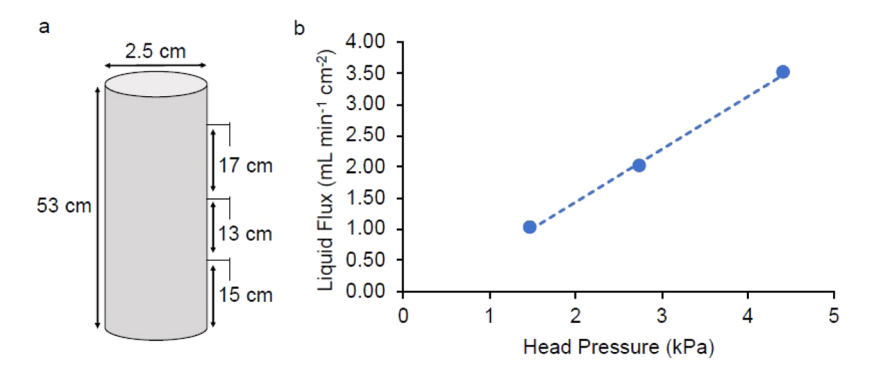


Figure 6. (a) Schematic of the glass-blown fluid flow apparatus that rests atop scaffolds for flow measurement. Outlets at heights 15, 28, and 45 cm from the bottom of the tube allow for flow measurements at constant liquid heights, thus constant head pressures (1.5, 2.7, and 4.4 kPa). (b) Average water flux through scaffolds over 100 min (1.0 ± 0.3 , 2.0 ± 0.4 , and 3.5 ± 1.0 mL min⁻¹ cm⁻², respectively) at three flow apparatus heights. Increasing water height corresponds with increasing head pressure. The dotted line is meant as a guide to the eye. Reported values were averaged from one flow measurement at each head pressure through three different three-molar scaffolds (nine measurements total).

Strength Measurement

Once dried, scaffolds at each concentration were subjected to uniaxial compressive measurements. Young's modulus and yield strength increased with each silicic acid concentration increase from one- to three-molar starting material (Figures 5 and S3). Under uniaxial compressive stress, the three-molar scaffold has a superior average Young's modulus of 455 ± 34 kPa and yield strength of 215 ± 10 kPa.

Liquid Flow Measurement

Liquid flows uniaxially through the scaffold's highly anisotropic pores. Using a simple apparatus (Figure 6a), flow characteristics of the finished three-molar product were probed at constant head pressures. A volumetric flux of water of 3.5 ± 1.0 mL min⁻¹ cm⁻² at 4.4 kPa head pressure was maintained for over 100 min without observable compromise of pore structure (Figures 6b and S4).

DISCUSSION

Highly Consolidated Walls

Combining freeze-casting with conventional sol-gel chemistry provides ideal pore morphologies for moderate-pressure, aqueous liquid flow applications. 4,19,20 Shown in the crosssectional micrograph (Figure 1a), scaffold pores are closed polygons in two dimensions. The longitudinal section micrograph (Figure 1b) reveals a large channel length-todiameter ratio. The consistent top-to-bottom microstructure of the third dimension of most pores means that the liquid entering a pore at the top of the scaffold likely exits via that same pore; in this way, the silica scaffold resembles a bundle of straws. Transverse section micrographs from the top, middle, and bottom of the same scaffold (Figure 2) corroborate the claim that pores remain consistent along the entire height of the sample, marking a key advancement relative to previously reported monoliths. Scaffolds prepared by this method can be utilized top-to-bottom without sacrificing material due to nonsteady-state freezing. Here, it is shown that a three-molar solution and fast freezing are required to generate uniform, straight pores.

Below three-molar concentration, the scaffold shows many lamellar structures (Figure 3), lacking cross-connections. Lack of cross-connections is deleterious to mechanical strength (Figure 5). The large aspect ratio of the pore diameters of one-and two-molar samples indicates there was not enough silicic

acid in solution to form smaller, more regular pores like those observed in the three-molar cross section. Wall volume calculations assuming the observed 10 $\mu \rm m$ pore wall thickness and 30 $\mu \rm m \times 65~\mu \rm m$ pore openings indicate that three-molar starting material provides sufficient silica monomer volume to yield consolidated scaffold walls. By this estimate, a two-molar starting material concentration would yield unconsolidated walls, as evidenced by the larger-perimeter two-dimensional pores in Figure 3. In aqueous applications, the three-molar, tens-of-microns-sized pores provide a suitable balance between maintaining high-deposition-area-to-volume ratio required of a substrate for functionalization and mitigating high Laplace pressure generated by surface tension. 23,32

Optimal Drying Method

The scaffold drying method was selected for optimal scaffold strength and pore morphology. Air-drying and lyophilization provided negligible strength and yielded un-handleable, disintegrating scaffolds. Leaving water in the scaffold and lyophilizing resulted in significant distortion, shrinkage, and inferior mechanical strength as water surface tension pulled smaller pores together. Oven-baking (calcination) at temperatures 300-800 °C provided significant strength yet caused considerable scaffold shrinkage, making scaffolds unusable. Supercritical drying (SCD) was chosen (Figure 4) as a wellsuited compromise to protect the morphology imparted via freeze-casting while increasing mechanical strength. Compared to lyophilization, SCD offers a 10³-10⁴ reduction in energy consumption during the drying step. Any unreacted silicic acid in smaller pores consolidates during SCD, resulting in a scaffold with reasonable mechanical strength. The strength provided by SCD generally does not exceed that provided by calcination. However, calcination of a microstructured product causes significant pore collapse, severely inhibiting function as a liquid flow device. 31,33 Supercritical drying allows handling the product without damage and yields improved freeze-cast silicaceous products for liquid flow applications 10 relative to freeze drying and calcination.

Mechanical Properties

Young's modulus and yield strength support the claim that only three-molar scaffolds have sufficiently consolidated walls (Figures 5b and S3). Under uniaxial compressive stress, the three-molar scaffold has a superior average Young's modulus of 455 ± 34 kPa and yield strength of 215 ± 10 kPa compared with one- and two-molar scaffolds. Freeze-cast glassy and

Table 1. Mechanical Properties of Freeze-Cast Silica Monoliths^a

inorganic/ organic	material	Young's modulus in compression (kPa)	yield strength in compression (kPa)	reference
purely inorganic	robust, reproducible silica scaffold	455 ± 34	215 ± 10	this report
purely inorganic	titania-silica "microhoneycomb"	not reported	40	Urkasame et al. ⁴
purely inorganic	macroporous silica "microhoneycomb"	not reported	100	Mukai et al. ³⁷
organic additives	silica-silk fibroin bioaerogel "silica-SF-10-66"	424,000	360	Maleki et al. ¹⁰
organic additives	macroporous silica scaffold with organic linkages	27 ± 0.7	not reported	Chatterjee et al. ²³
organic additives	soft silica scaffold with organic linkages	24	not reported	Rajamanickam et al. ²⁵

[&]quot;Among purely inorganic silica-based anisotropic scaffolds, this report contains the most mechanically robust product. While organic additives can reinforce scaffold walls and provide increased mechanical strength, incorporation of organics can also lead to scaffold degradation depending upon the desired application or functionalization.

ceramic-like materials demonstrate brittle intergranular fracture under compressive stress with relatively high Young's moduli. 34,35 To our knowledge, no other purely silica scaffold (Table 1) with highly anisotropic porosity reported is stronger under compression without calcination, which regularly increases Young's modulus from the order of 10^3-10^5 to 10^6-10^9 Pa. 9,25 Organic additives can increase the durability of freeze-cast materials (Table 1). 10,25,36 However, for applications involving harsh chemicals or irradiation, organic additives compromise the corrosion- and UV-resistance of the substrate. The ability to withstand harsh chemicals, UV irradiation, and moderate handling are often key factors in whether microreactors can be implemented outside of a laboratory setting.

Pore Sizes Ideal for Liquid Flow

Pore anisotropy and diameter are controlled during synthesis to produce scaffolds that facilitate liquid flux at low head pressures. For scaffolds with $10-100 \mu m$ pore diameters, we estimate Laplace pressures of 0.03-0.28 atm. Pores on the order of tens of microns allow scaffolds to endure liquid flow without destructive pore rupture, unlike glassy materials with pores smaller than three microns. Experimentally, scaffolds synthesized by this method can sustain $3.5 \pm 1.0 \text{ mL min}^{-1}$ cm⁻² volumetric flux of water with 4.4 kPa head pressure (Figure 6) and can likely sustain relatively faster rates and higher head pressures without device damage; flux is linearly dependent on applied head pressure. Anisotropic scaffold macropores with an equivalent diameter of 47 μ m at these three head pressures result in an estimated Reynolds number less than 0.02 for water. This small Reynolds number indicates laminar flow, which reduces strain on pore walls. With laminar flow, the estimated diffusion time for solute molecules to travel from the center of the pore to a scaffold wall is on the order of milliseconds. This allows sufficient time for multiple interactions between liquid-phase moieties and functionalized scaffold walls during transit.

Anisotropic pores in the ice-templated scaffold allow for lower-pressure, higher-volume liquid flow than spongy materials with torturous liquid paths despite similar pore sizes. ^{23,38} This silica scaffold has flow capabilities and head pressures similar to those reported for other anisotropic microreactors. ⁴ The flow capabilities of this scaffold enable its use in combination batch-flow applications or in continuous flow settings, and its translucency is useful in applications where adsorbed moieties are activated by visible or UV light (Discussion S1, Figures S5 and S6).

CONCLUSIONS

The reported silica scaffold represents an innovation in the way water glass can be transformed to generate a robust, large deposition-area support for diverse liquid flow applications. The novelty of this reproducible support hinges on chemical and physical processing steps: acidifying a dilute solution of sodium silicate, concentrating via rotary evaporation, freezecasting, and supercritical drying. With a Young's Modulus of 455 ± 34 kPa, a yield strength of 215 ± 10 kPa, and the ability to pass water at 3.5 \pm 1.0 mL min⁻¹ cm⁻² with 4.4 kPa head pressure, this flow-enabling substrate can potentially be incorporated into heterogeneous catalysis, energy storage, separations, and biomedical applications. Supercritical drying and rotary evaporation are already incorporated in commercial processes, and freeze-casting could easily be commercialized, so it is likely that this scaffold preparation method could be scaled up in a manufacturing process. The reported substrate is unique for its reproducible structure, strength, and flow characteristics, bridging the divide between lab-scale and industrial-scale applications.

ASSOCIATED CONTENT

Supporting Information

The Supporting Information is available free of charge at https://pubs.acs.org/doi/10.1021/acsaenm.3c00149.

Freeze front velocity effect on pore size (Table S1); micrographs demonstrating the effect of freeze front velocity on pore cross section (Figure S1); dynamic light scattering of basic sodium silicate starting material (Figure S2); stress—strain curves for one-, two-, and three-molar scaffolds (Figure S3); water flow rate as a function of time at 1.47 kPa constant head pressure (Figure S4); scaffold transmission measurements and optical properties (Discussion S1); photograph of scaffold transmittance measurement apparatus (Figure S5); and percent transmittance through three-molar scaffolds in water and air at three visible wavelengths (Figure S6) (PDF)

AUTHOR INFORMATION

Corresponding Author

Mary Jane Shultz – Department of Chemistry, Pearson Chemical Laboratory, Tufts University, Medford, Massachusetts 02155, United States; orcid.org/0000-0001-5625-1675; Email: Mary.Shultz@Tufts.edu

Authors

- Rebecca G. Davies Department of Chemistry, Pearson Chemical Laboratory, Tufts University, Medford, Massachusetts 02155, United States; orcid.org/0000-0002-4135-3713
- Allyson E. MacInnis Department of Chemistry, Pearson Chemical Laboratory, Tufts University, Medford, Massachusetts 02155, United States
- Patrick J. Bisson Department of Chemistry, Pearson Chemical Laboratory, Tufts University, Medford, Massachusetts 02155, United States; Present Address: Cambridge Polymer Group, Inc., 100 TradeCenter Drive, Suite 200, Woburn, MA 01801, United States

Complete contact information is available at: https://pubs.acs.org/10.1021/acsaenm.3c00149

Author Contributions

R.G.D. and A.E.M. contributed equally.

The authors declare no competing financial interest.

ACKNOWLEDGMENTS

Funding from the Provost Office, Tufts University Launchpad Accelerator 2022, is gratefully acknowledged. R.G.D. gratefully acknowledges partial funding from the U.S. Department of Energy, Basic Energy Sciences (DE-SC0020258) and the National Science Foundation (CHE-1807913). A.E.M. gratefully acknowledges partial support by the Air Force Office of Scientific Research Multidisciplinary University Research Initiative (FA9550-20-1-0351). The authors thank Yu Yan and the Thomas Lab at Tufts University for their collection of dynamic light scattering data.

REFERENCES

- (1) Rouquerol, J.; Avnir, D.; Fairbridge, C. W.; Everett, D. H.; Haynes, J. M.; Pernicone, N.; Ramsay, J. D.; Sing, K. S.; Unger, K. K. Recommendations for the Characterization of Porous Solids (Technical Report). *Pure Appl. Chem.* **1994**, *66*, 1739–1758.
- (2) Velev, O. D.; Jede, T. A.; Lobo, R. F.; Lenhoff, A. M. Porous Silica via Colloidal Crystallization. *Nature* **1997**, *389*, 447–448.
- (3) Sachse, A.; Galarneau, A.; Fajula, F.; Di Renzo, F.; Creux, P.; Coq, B. Functional Silica Monoliths with Hierarchical Uniform Porosity as Continuous Flow Catalytic Reactors. *Microporous Mesoporous Mater.* **2011**, *140*, 58–68.
- (4) Urkasame, K.; Yoshida, S.; Takanohashi, T.; Iwamura, S.; Ogino, I.; Mukai, S. R. Development of TiO₂—SiO₂ Photocatalysts Having a Microhoneycomb Structure by the Ice Templating Method. *ACS Omega* **2018**, *3*, 14274—14279.
- (5) Buga, M.-R.; Spinu-Zaulet, A. A.; Ungureanu, C. G.; Mitran, R.-A.; Vasile, E.; Florea, M.; Neatu, F. Carbon-Coated SiO₂ Composites as Promising Anode Material for Li-Ion Batteries. *Molecules* **2021**, *26*, 4531.
- (6) Poryvaev, A. S.; Gjuzi, E.; Yazikova, A. A.; Polyukhov, D. M.; Albrekht, Y. N.; Efremov, A. A.; Kudriavykh, N. A.; Yanshole, V. V.; Hoffmann, F.; Fröba, M.; Fedin, M. V. Blatter Radical-Decorated Silica as a Prospective Adsorbent for Selective NO Capture from Air. ACS Appl. Mater. Interfaces 2023, 15, 5191–5197.
- (7) Su, X. D.; Tao, J.; Chen, S.; Xu, P.; Wang, D.; Teng, Z. G. Uniform Hierarchical Silica Film with Perpendicular Macroporous

- Channels and Accessible Ordered Mesopores for Biomolecule Separation. Chin. Chem. Lett. 2019, 30, 1089-1092.
- (8) Zhao, D.; Feng, J.; Huo, Q.; Melosh, N.; Fredrickson, G. H.; Chmelka, B. F.; Stucky, G. D. Triblock Copolymer Syntheses of Mesoporous Silica with Periodic 50 to 300 Angstrom Pores. *Science* **1998**, 279, 548–552.
- (9) Choi, Y.; Jeong, J. H.; Kim, J. Mechanically Enhanced Hierarchically Porous Scaffold Composed of Mesoporous Silica for Host Immune Cell Recruitment. *Adv. Healthcare Mater.* **2017**, *6*, No. 1601160.
- (10) Maleki, H.; Shahbazi, M.-A.; Montes, S.; Hosseini, S. H.; Eskandari, M. R.; Zaunschirm, S.; Verwanger, T.; Mathur, S.; Milow, B.; Krammer, B.; Hüsing, N. Mechanically Strong Silica-Silk Fibroin Bioaerogel: A Hybrid Scaffold with Ordered Honeycomb Micromorphology and Multiscale Porosity for Bone Regeneration. ACS Appl. Mater. Interfaces 2019, 11, 17256–17269.
- (11) Iqbal, M. N.; Robert-Nicoud, G.; Ciurans-Oset, M.; Akhtar, F.; Hedin, N.; Bengtsson, T. Mesoporous Silica Particles Retain Their Structure and Function while Passing through the Gastrointestinal Tracts of Mice and Humans. ACS Appl. Mater. Interfaces 2023, 15, 9542–9553.
- (12) Wang, D. Y.; Caruso, R. A.; Caruso, F. Synthesis of Macroporous Titania and Inorganic Composite Materials from Coated Colloidal Spheres A Novel Route to Tune Pore Morphology. *Chem. Mater.* **2001**, *13*, 364–371.
- (13) Zanardo, D.; Forghieri, G.; Tieuli, S.; Ghedini, E.; Menegazzo, F.; Di Michele, A.; Cruciani, G.; Signoretto, M. Effects of SiO₂-Based Scaffolds in TiO₂ Photocatalyzed CO₂ Reduction. *Catal. Today* **2022**, 387. 54–60.
- (14) Tillotson, T. M.; Hrubesh, L. W. Transparent Ultralow-Density Silica Aerogels Prepared by a Two-Step Sol-Gel Process. *J. Non-Cryst. Solids* **1992**, *145*, 44–50.
- (15) Zhao, L.; Bhatia, B.; Yang, S.; Strobach, E.; Weinstein, L. A.; Cooper, T. A.; Chen, G.; Wang, E. N. Harnessing Heat Beyond 200 °C from Unconcentrated Sunlight with Nonevacuated Transparent Aerogels. ACS Nano 2019, 13, 7508–7516.
- (16) Hubadillah, S. K.; Othman, M. H. D.; Matsuura, T.; Rahman, M. A.; Jaafar, J.; Ismail, A. F.; Amin, S. Z. M. Green Silica-Based Ceramic Hollow Fiber Membrane for Seawater Desalination via Direct Contact Membrane Distillation. Sep. Purif. Technol. 2018, 205, 22–31.
- (17) Jaisingh, A.; Goel, V.; Kapur, G. S.; Nebhani, L. Reactive Compatibilization of Impact Copolymer Polypropylene and Organically Modified Mesoporous Silica to Prepare Composites Possessing Enhanced Mechanical Properties. *ACS Appl. Eng. Mater.* **2023**, *1*, 877–893.
- (18) Kim, J.-W.; Tazumi, K.; Okaji, R.; Ohshima, M. Honeycomb Monolith-Structured Silica with Highly Ordered, Three-Dimensionally Interconnected Macroporous Walls. *Chem. Mater.* **2009**, *21*, 3476–3478.
- (19) Mukai, S. R.; Nishihara, H.; Tamon, H. Porous Properties of Silica Gels with Controlled Morphology Synthesized by Unidirectional Freeze-Gelation. *Microporous Mesoporous Mater.* **2003**, *63*, 43–51.
- (20) Nishihara, H.; Mukai, S. R.; Yamashita, D.; Tamon, H. Ordered Macroporous Silica by Ice Templating. *Chem. Mater.* **2005**, *17*, 683–689.
- (21) Suh, D. J.; Park, T. J.; Han, H. Y.; Lim, J. C. Synthesis of High-Surface-Area Zirconia Aerogels with a Well-Developed Mesoporous Texture Using CO₂ Supercritical Drying. *Chem. Mater.* **2002**, *14*, 1452–1454.
- (22) Deville, S.; Saiz, E.; Nalla, R. K.; Tomsia, A. P. Freezing as a Path to Build Complex Composites. *Science* **2006**, *311*, 515–518.
- (23) Chatterjee, S.; Potdar, A.; Kuhn, S.; Kumaraswamy, G. Preparation of Macroporous Scaffolds with Holes in Pore Walls and Pressure Driven Flows through Them. *RSC Adv.* **2018**, *8*, 24731–24739.

- (24) Nishihara, H.; Mukai, S. R.; Shichi, S.; Tamon, H. Preparation of titania-silica cryogels with controlled shapes and photocatalysis through unidirectional freezing. *Mater. Lett.* **2010**, *64*, 959–961.
- (25) Rajamanickam, R.; Kumari, S.; Kumar, D.; Ghosh, S.; Kim, J. C.; Tae, G.; Sen Gupta, S.; Kumaraswamy, G. Soft Colloidal Scaffolds Capable of Elastic Recovery after Large Compressive Strains. *Chem. Mater.* **2014**, *26*, 5161–5168.
- (26) Zhang, H.; Hussain, I.; Brust, M.; Butler, M. F.; Rannard, S. P.; Cooper, A. I. Aligned Two- and Three-Dimensional Structures by Directional Freezing of Polymers and Nanoparticles. *Nat. Mater.* **2005**, *4*, 787–793.
- (27) Genov, G. Device for Measuring Stress-Strain Curves of Soft Materials: A Poor Man's Solution 2018.
- (28) Brinker, C. J. Hydrolysis and Condensation of Silicates: Effects on Structure. *J. Non-Cryst. Solids* **1988**, *100*, 31–50.
- (29) Iler, R. K. 4. Colloidal Silica-Concentrated Sols. In *Chemistry of Silica Solubility, Polymerization, Colloid and Surface Properties and Biochemistry*; John Wiley & Sons, 1979; pp 375–378.
- (30) Nelson, I.; Naleway, S. E. Intrinsic and Extrinsic Control of Freeze Casting. J. Mater. Res. Technol. 2019, 8, 2372-2385.
- (31) García-González, C.; Camino-Rey, M. C.; Alnaief, M.; Zetzl, C.; Smirnova, I. Supercritical Drying of Aerogels Using CO₂: Effect of Extraction Time on the End Material Textural Properties. *J. Supercrit. Fluids* **2012**, *66*, 297–306.
- (32) Chao, C.; Xu, X.; Kwelle, S. O.; Fan, X. Significance of Gas-Liquid Interfaces for Two-Phase Flows in Micro-Channels. *Chem. Eng. Sci.* **2018**, *192*, 114–125.
- (33) Putz, F.; Waag, A.; Balzer, C.; Braxmeier, S.; Elsaesser, M. S.; Ludescher, L.; Paris, O.; Malfait, W. J.; Reichenauer, G.; Hüsing, N. The Influence of Drying and Calcination on Surface Chemistry, Pore Structure and Mechanical Properties of Hierarchically Organized Porous Silica Monoliths. *Microporous Mesoporous Mater.* **2019**, 288, No. 109578.
- (34) Liu, H.; Li, L.; Li, J.; Guo, A.; Hu, X.; Du, H. Mechanical Response and Failure Behavior of Fiber Enforced Porous Ceramics by Directional Freeze-Casting. *Ceram. Int.* **2021**, *47*, 8593–8600.
- (35) Seuba, J.; Deville, S.; Guizard, C.; Stevenson, A. J. Mechanical Properties and Failure Behavior of Unidirectional Porous Ceramics. *Sci. Rep.* **2016**, *6*, No. 24326.
- (36) Loy, D. A.; Russick, E. M.; Yamanaka, S. A.; Baugher, B. M.; Shea, K. J. Direct Formation of Aerogels by Sol—Gel Polymerizations of Alkoxysilanes in Supercritical Carbon Dioxide. *Chem. Mater.* **1997**, 9, 2264—2268
- (37) Mukai, S. R.; Onodera, K.; Yamada, I. Studies on the Growth of Ice Crystal Templates During the Synthesis of a Monolithic Silica Microhoneycomb Using the Ice Templating Method. *Adsorption* **2011**, *17*, 49–54.
- (38) Vanson, J.-M.; Boutin, A.; Klotz, M.; Coudert, F.-X. Transport and Adsorption Under Liquid Flow: the Role of Pore Geometry. *Soft Matter* **2017**, *13*, 875–885.

NOTE ADDED AFTER ISSUE PUBLICATION

Due to a production error, the original version of the article has been updated to reflect the originally agreed upon authorship order and the originally agreed upon author contribution line. The corrected version was reposted on August 31, 2023.